Ultra-compact, low RF power, 10 Gb/s silicon Mach-Zehnder modulator

William M. J. Green, Michael J. Rooks, Lidija Sekaric, and Yurii A. Vlasov

IBM Thomas J. Watson Research Center, Yorktown Heights, NY 10598, USA
wgreen@us.ibm.com
http://www.research.ibm.com/photonics

Abstract: Silicon p^+-i-n^+ diode Mach-Zehnder electrooptic modulators having an ultra-compact length of 100 to 200 μm are presented. These devices exhibit high modulation efficiency, with a $V_\pi \cdot L$ figure of merit of 0.36 V-mm. Optical modulation at data rates up to 10 Gb/s is demonstrated with low RF power consumption of only 5 pJ/bit.

OCIS codes: (250.7360) Waveguide modulators; (250.5300) Photonic integrated circuits.

References and links

1. A. Shacham, K. Bergman, and L. P. Carloni, "On the design of a photonic network on chip," in *Proceedings of the First IEEE International Symposium on Networks-on-Chips* (Institute of Electrical and Electronics Engineers, New York, 2007), pp. 53-64.
2. D. A. B. Miller, "Optical interconnects to silicon," IEEE J. Sel. Top. Quantum Electron. **6**, 1312-1317 (2000).
3. R. A. Soref and B. R. Bennett, "Electrooptical effects in silicon," IEEE J. Quantum Electron. **23**, 123-129 (1987).
4. R. A. Soref and J. P. Lorenzo, "All-silicon active and passive guided-wave components for λ = 1.3 and 1.6 μm," IEEE J. Quantum Electron. **22**, 873-879 (1986).
5. G. V. Treyz, P. G. May, and J.-M. Halbout, "Silicon Mach-Zehnder waveguide interferometers based on the plasma dispersion effect," Appl. Phys. Lett. **59**, 771-773 (1991).
6. G. V. Treyz, P. G. May, and J.-M. Halbout, "Silicon optical modulators at 1.3 μm based on free-carrier absorption," IEEE Electron Device Lett. **12**, 276-278 (1991).
7. C. K. Tang and G. T. Reed, "Highly efficient optical phase modulator in SOI waveguides," Electron. Lett. **31**, 451-452 (1995).
8. P. Dainesi, A. Kung, M. Chabloz, A. Lagos, P. Fluckiger, A. Ionescu, P. Fazan, M. Declerq, P. Renaud, and P. Robert, "CMOS compatible fully integrated Mach-Zehnder interferometer in SOI technology," IEEE Photon. Technol. Lett. **12**, 660-662 (2000).
9. Y. Vlasov and S. McNab, "Losses in single-mode silicon-on-insulator strip waveguides and bends," Opt. Express **12**, 1622-1631 (2004).
10. Q. Xu, S. Manipatruni, B. Schmidt, J. Shakya, and M. Lipson, "12.5 Gbit/s carrier-injection-based silicon micro-ring silicon modulators," Opt. Express **15**, 430-436 (2007).
11. Q. Xu, B. Schmidt, S. Pradhan, and M. Lipson, "Micrometre-scale silicon electro-optic modulator," Nature **435**, 325-327 (2005).
12. C. Li, L. Zhou, and A. W. Poon, "Silicon microring carrier-injection-based modulators/switches with tunable extinction ratios and OR-logic switching by using waveguide cross-coupling," Opt. Express **15**, 5069-5076 (2007).
13. A. Liu, R. Jones, L. Liao, D. Samara-Rubio, D. Rubin, O. Cohen, R. Nicolaescu, and M. Paniccia, "A high-speed silicon optical modulator based on a metal-oxide-semiconductor capacitor," Nature **427**, 615-618 (2004).
14. L. Liao, D. Samara-Rubio, M. Morse, A. Liu, D. Hodge, D. Rubin, U. Keil, and T. Franck, "High speed silicon Mach-Zehnder modulator," Opt. Express **13**, 3129-3135 (2005).
15. A. Liu, L. Liao, D. Rubin, H. Nguyen, B. Ciftcioglu, Y. Chetrit, N. Izhaky, and M. Paniccia, "High-speed optical modulation based on carrier depletion in a silicon waveguide," Opt. Express **15**, 660-668 (2007).
16. B. Analui, D. Guckenberger, D. Kucharski, and A. Narasimha, "A fully integrated 20-Gb/s optoelectronic transceiver implemented in a standard 0.13-μm CMOS SOI technology," IEEE J. Solid-State Circuits **41**, 2945-2955 (2006).
17. W. M. J. Green, M. J. Rooks, L. Sekaric, and Y. A. Vlasov, "Ultra-compact, low RF power, 10 Gb/s silicon Mach-Zehnder modulator," in *Proceedings of the 20th Annual Meeting of the IEEE Lasers & Electro-*

#87799 - $15.00 USD Received 21 Sep 2007; revised 6 Nov 2007; accepted 7 Nov 2007; published 6 Dec 2007

Optics Society (Institute of Electrical and Electronics Engineers, New York, 2007), Postdeadline paper PD1.2.

18. L. Sekaric, S. J. McNab, and Y. A. Vlasov, "Y-splitters in photonic wires and photonic crystal waveguides," presented at the VI Symposium on Photonic and Electromagnetic Crystal Structures, Crete, Greece, 19-24 June 2005. http://www.research.ibm.com/photonics/posters/splittters_pecsvi.pdf
19. S. McNab, N. Moll, and Y. Vlasov, "Ultra-low loss photonic integrated circuit with membrane-type photonic crystal waveguides," Opt. Express **11**, 2927-2939 (2003).
20. C. A. Barrios, V. R. Almeida, R. Panepucci, and M. Lipson, "Electrooptic modulation of silicon-on-insulator submicrometer-size waveguide devices," J. Lightwave Technol. **21**, 2332-2339 (2003).
21. F. Gardes, G. Reed, N. Emerson, and C. Png, "A sub-micron depletion-type photonic modulator in Silicon On Insulator," Opt. Express **13**, 8845-8854 (2005).
22. H. Stark, F. B. Tuteur, and J. B. Anderson, *Modern Electrical Communications*, (Prentice Hall, Englewood Cliffs, 1988).
23. S. Haykin, *Communication Systems*, (Wiley, New York, 1994).
24. T. Barwicz, H. Byun, F. Gan, C. W. Holzwarth, M. A. Popovic, P. T. Rakich, M. R. Watts, E. P. Ippen, F. X. Kartner, H. I. Smith, J. S. Orcutt, R. J. Ram, V. Stojanovic, O. O. Olubuyide, J. L. Hoyt, S. Spector, M. Geis, M. Grein, T. Lyszczarz, and J. U. Yoon, "Silicon photonics for compact energy-efficient interconnects," J. Opt. Netw. **6**, 63-73 (2007).
25. F. Gan, S. J. Spector, M. W. Geis, M. E. Grein, R. T. Schulein, J. U. Yoon, T. M. Lyszczarz, and F. X. Kartner, "Compact, low-power, high-speed silicon electro-optic modulator," in *Conference on Lasers and Electro-Optics/Quantum Electronics and Laser Science*, Technical Digest (CD) (Optical Society of America, 2007), paper CTuQ6.

1. Introduction

A primary factor driving the high level of research interest in the silicon photonics platform originates from this system's intrinsic compatibility with CMOS electronics. The ability to leverage the mature manufacturing infrastructure behind this technology creates the potential for integrating advanced silicon-based waveguide networks as high-bandwidth on-chip optical interconnects for high performance computing applications [1, 2]. One of the principal components required within any optical communication link is the electrooptic modulator, which serves the function of encoding an optical carrier wave with a high speed electronic data signal.

Silicon modulators based upon free carrier electrooptic effects [3] have continued to evolve over the past two decades. Beginning with epitaxial silicon-on-silicon substrates, in which a lightly doped Si layer on a heavily doped Si substrate served as the optical waveguide [4], rib waveguide Mach-Zehnder interferometers [5] and electroabsorption modulators [6] using embedded p^+-i-n^+ diodes for charge injection were demonstrated. Modulator development subsequently progressed toward the use of silicon-on-insulator (SOI) substrates [7, 8], where high index contrast optical confinement has enabled the use of compact low-loss waveguide bends (radius < 5 μm) [9], ultimately resulting in the deeply scaled nanophotonic wire devices frequently used today.

A recent example of the extent to which SOI optical modulators have been scaled is illustrated by devices based upon the micro-ring resonator. Charge injection based p^+-i-n^+ diode modulators with ultra-compact footprint (approximately 0.0002 mm^2) have been realized using high quality factor optical micro-resonators [10-12]. The compact nature of these devices is made possible on account of the enhancement of modulation efficiency near sharp spectral resonances. However, it is precisely this same resonant enhancement which simultaneously makes these structures highly sensitive to small variations in bias conditions, operating temperature, and fabrication tolerances.

In contrast, the familiar Mach-Zehnder modulator (MZM) geometry possesses the advantage of broadband spectral operation and improved tolerance to environmental and process fluctuations. Recent studies of high-performance SOI MZMs have included metal-oxide-semiconductor (MOS) capacitor [13, 14] and p-n diode [15, 16] driven devices. However, the large footprint occupied by these modulators, having active lengths on the order of several millimeters, restricts their use within highly integrated ultra-compact on-chip interconnect systems, where it is likely that hundreds if not thousands of modulators will be

#87799 - $15.00 USD Received 21 Sep 2007; revised 6 Nov 2007; accepted 7 Nov 2007; published 6 Dec 2007

required on a single die. An ultra-compact MZM device would therefore be an indispensable choice for many on-chip applications, including filtering and switching functions in addition to optical modulation.

In this report, we demonstrate several ultra-compact (100 to 200 μm length), low RF power (5 pJ/bit), high speed SOI MZM devices, capable of operating at data rates up to 10 Gb/s [17]. Despite the conventionally held view that a non-resonant modulator such as the MZM must naturally be designed with a long optical interaction length, the devices reported here demonstrate that it is indeed possible to design a high-performance ultra-compact MZM component with micron-scale dimensions, suitable for on-chip optical interconnect applications.

2. Design and fabrication

The ultra-compact MZM devices demonstrated here were designed using nanophotonic rib waveguides with embedded p^+-i-n^+ diodes as charge injection-based electrooptic phase shifters. A cross-sectional scanning electron microscope (SEM) image of the active waveguide structure is shown in Fig. 1(a). These rib waveguides were nominally 550 nm wide and 220 nm in height, with a 35 nm silicon slab providing a conductive path between the anode and cathode, for the injection of free carriers into the intrinsic waveguide core.

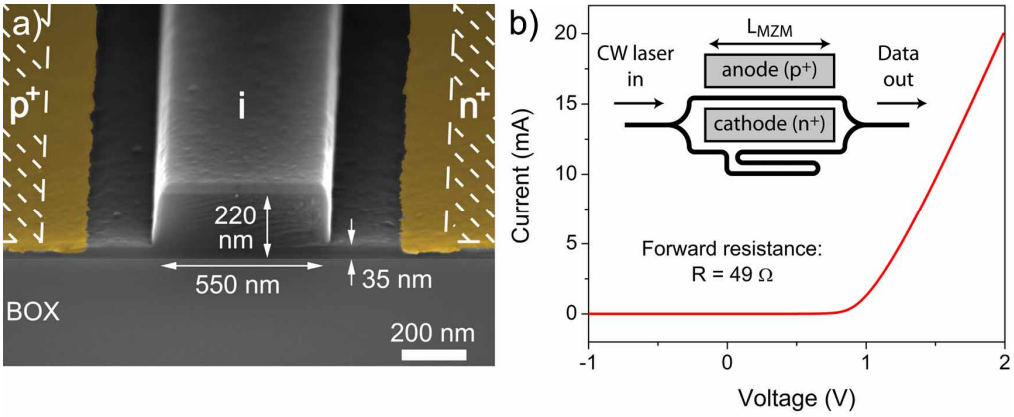

Fig. 1. (a). Cross-sectional scanning electron microscope image of the SOI p^+-i-n^+ diode nanophotonic rib waveguide used. The heavily doped p^+/n^+ regions are hatched, and the nickel silicide contact regions are highlighted in gold false color. A 25 nm layer of silicon dioxide remains on top of the rib waveguide. (b). Electrical I-V trace taken for a modulator with L_{MZM} = 100 μm, illustrating a low forward resistance of 49 Ω. Inset: Schematic of the asymmetric MZM device geometry fabricated.

In comparison with previously demonstrated SOI MZM devices, where much larger rib waveguides having cross-sectional areas on the order of 1 μm^2 or larger were employed, the ultra-compact cross-section of nanophotonic rib waveguides simultaneously confines both the injected free carriers and the fundamental TE_{00} mode profile to an effective area of approximately 0.12 μm^2. Localization of both photons and free carriers within such a small region produces two effects beneficial for efficient modulator performance. First, during each ON/OFF modulation cycle, the diode injection current is forced to flow through a cross-section only 220 nm in height, producing large changes in the free carrier density within the intrinsic rib waveguide core. Second, the ultra-compact modal cross-section assures nearly complete free carrier/optical mode overlap, resulting in large modulation of the modal effective index. Taken together, these two characteristics of p^+-i-n^+ diode nanophotonic rib waveguides lead to highly efficient operation as electrooptic phase shifters, enabling MZM devices requiring greatly reduced active length, as will be illustrated below.

#87799 - $15.00 USD Received 21 Sep 2007; revised 6 Nov 2007; accepted 7 Nov 2007; published 6 Dec 2007

Furthermore, while rib waveguides with larger dimensions require large radius bends (R > 20 μm) in order to avoid excessive bend losses, the nanophotonic rib waveguide yields ultra-compact low-loss bends with radii < 5 μm [9], as well as ultra-compact Y-junction splitters [18]. Therefore, the total footprint of MZM devices designed with nanophotonic rib waveguides is limited only by the length of the phase shifter section L_{MZM}, rather than the bend radius.

MZM devices with various p^+-i-n^+ diode phase shifter lengths L_{MZI} (as shown in Fig. 1(b) inset) were fabricated on a SOI substrate (p-type, resistivity 10 Ω-cm) having a 2 μm thick buried oxide layer. A series of aligned electron beam lithographic exposures was used to define rib waveguides, anode (boron, $p^+ \sim 1x10^{20}$ cm^{-3}) and cathode (phosphorus, $n^+ \sim 1x10^{20}$ cm^{-3}) implants, and ohmic contact pads using nickel silicide. The distance between the heavily doped regions (hatched areas in Fig. 1(a)) and the edges of the rib waveguide core was nominally 400 nm. However, the nickel silicide contact pads (highlighted in gold) were formed closer to the waveguide edges than intended, resulting in additional on-chip optical loss as will be described below. Finally, polymer spotsize converters were formed over SOI waveguide inverted tapers [19] for efficient coupling to tapered optical fibers, and device chips were cleaved for testing.

3. Experimental results and discussion

An electrical I-V curve obtained for a MZM with a 100 μm long active p^+-i-n^+ phase shifter region is shown in Fig. 1(b). Under typical high speed operating conditions, large current densities flow across the nanophotonic rib waveguide cross-section, as the p^+-i-n^+ diode is modulated between forward (ON) and reverse biased (OFF) states. Despite channeling of this current through the thin 35 nm silicon slab at the anode/cathode terminals, the forward differential resistance of 49 Ω illustrated in the figure indicates that low electrical impedance can be achieved, as necessary for matching to 50 Ω drive electronics and ensuring low power consumption. Furthermore, this measurement serves to emphasize that the high impedance observed previously (on the order of 10 kΩ) for comparable nanophotonic rib diode structures [10, 11] is not a fundamental limitation of the waveguide structure itself, but rather depends upon the dopant profile and contact resistance. In addition, the measured device exhibited a reverse leakage current of less than 10 nA, indicating that the reverse bias potential generates a large electric field localized across the depleted intrinsic region of the waveguide core, resulting in fast, efficient sweep-out of injected carriers. Finally, a reverse bias capacitance of 200 fF was measured, suggesting that this device has a high-frequency RC cutoff of approximately 16 GHz.

The spectral transmission characteristics of the MZM devices near λ = 1550 nm were characterized using a broadband LED light source polarized to excite the TE guided mode, and an optical spectrum analyzer. Interference fringes with a free spectral range (FSR) of 7.3 nm were observed, corresponding to a built-in 80 μm path length difference between the two branches of the MZM, as shown in the inset schematic of Fig. 1(b). A balanced MZM would be desirable to maximize the optical bandwidth of the device. However, for illustration purposes in this work, the presence of interference fringes assisted in distinguishing between thermooptic and electrooptic effects under low-frequency modulation, and in the measurement of extinction ratios.

A measured on-chip loss of 12 dB and relatively low extinction ratio of 6-10 dB originated primarily from metal losses caused by unintentional placement of the nickel silicide contact pads approximately 200 nm away from the edges of the rib waveguide, as shown in Fig. 1(a). However, these losses do not present a fundamental limitation. Increasing the distance between the lossy contact pads and the waveguide without moving the highly doped p+ and n+ regions would result in nearly identical electrical performance, while significantly decreasing on-chip loss and improving extinction.

Measurements of the figure of merit $V_\pi \cdot L$ and data transmission, described below, were carried out by coupling light from a TE-polarized tunable laser into the MZM device and

#87799 - $15.00 USD Received 21 Sep 2007; revised 6 Nov 2007; accepted 7 Nov 2007; published 6 Dec 2007

tuning to a quadrature point near λ = 1550 nm. The modulated output was amplified by an erbium doped fiber amplifier (EDFA), and detected using a 15 GHz optical receiver connected to a digital communications analyzer (DCA) electrical module with 20 GHz bandwidth.

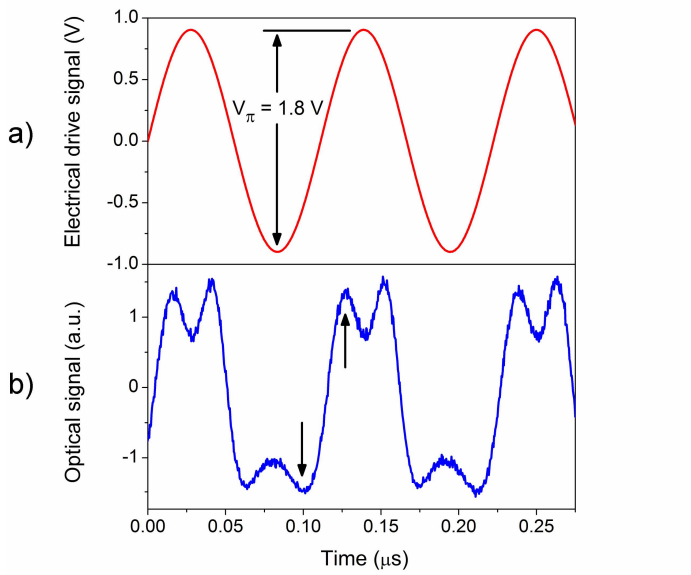

Fig. 2. (a). Application of a 9 MHz sinusoidal voltage with peak-to-peak amplitude of V_π = 1.8 V to a L_{MZI} = 200 μm modulator (V_{bias} = 1.8 V). (b) The resulting half-period of sinusoidal optical modulation occurring between the maxima/minima indicated by arrows illustrates a $V_\pi \cdot L$ product of 0.36 V-mm.

Measurement of V_π under AC conditions permits observation of the *intrinsic* free carrier electrooptic efficiency of the MZM, which under DC operating conditions can be masked to a great extent by slow thermooptic effects. The voltage V_π required to produce a carrier injection-induced π phase shift was measured by applying a 9 MHz sinusoidal electrical drive signal, as shown in Fig. 2(a), to a L_{MZM} = 200 μm long modulator, under a forward bias conditions (V_{bias} = 1.8 V). The drive amplitude was increased until the slope of the modulated optical signal changed sign at the peaks/troughs of the drive waveform, as illustrated in Fig. 2(b). A complete half-period of optical modulation (between the two arrows in Fig. 2(b), for example) was observed for a peak-to-peak applied voltage of V_π = 1.8 V, leading to a MZM figure of merit of $V_\pi \cdot L$ = 0.36 V-mm. This value of V_π resulted from a change of $\Delta n \sim 4 \times 10^{-3}$ in the modal effective index within the 200 μm long phase shifter, corresponding to injection of a free electron-hole pair density of approximately 1.5×10^{18} cm^{-3}. In comparison with recently published silicon Mach-Zehnder modulators [13-16], the measured $V_\pi \cdot L$ figure of merit represents a 100x improvement in the electrooptic modulation efficiency. Furthermore, while previous MZM devices have required lengths on the order of several millimeters to achieve a significant phase shift, the present device demonstrates a π phase shift with an active section approximately 20x to 50x shorter. As discussed above, the observed improvement in performance originates from simultaneous confinement of both the injected free carriers and the mode profile within the ultra-compact 0.12 μm^2 cross-section of the SOI nanophotonic rib waveguide structure.

The high frequency performance of charge injection-based silicon electrooptic modulators is limited by the slow recombination dynamics of minority carriers injected into the p^+-i-n^+ diode junction under forward bias [20], while the depletion of injected carriers in reverse bias

#87799 - $15.00 USD Received 21 Sep 2007; revised 6 Nov 2007; accepted 7 Nov 2007; published 6 Dec 2007

can occur on much shorter time scales [21]. The large asymmetry between the rise and fall time of the carrier concentration within the nanophotonic rib waveguide waveguide, and accordingly the free carrier induced phase shift, results in significant intersymbol interference (ISI) which limits the maximum data rate to approximately 1 Gb/s [11]. However, pre-emphasis is a commonly used technique for mitigating signal degradation in systems suffering from ISI [22, 23], and was used to demonstrate high speed operation of the ultra-compact MZM devices described here. A NRZ electrical drive signal from a pseudo-random bit sequence (PRBS) generator was pre-emphasized in similar manner to that described by Xu et. al. [10]. For all experiments discussed below, the modulator drive signal was composed of a 1.2 V peak-to-peak NRZ pattern with pre-emphasis pulses having 3.5 V peak amplitude occurring at each transition between a 1-bit and a 0-bit. A bit sequence from a 5 Gb/s pre-emphasized drive signal is shown in Fig. 3(a), while Fig. 3(b) illustrates the corresponding modulated optical output when the drive signal was applied to a 100 μm long MZM device.

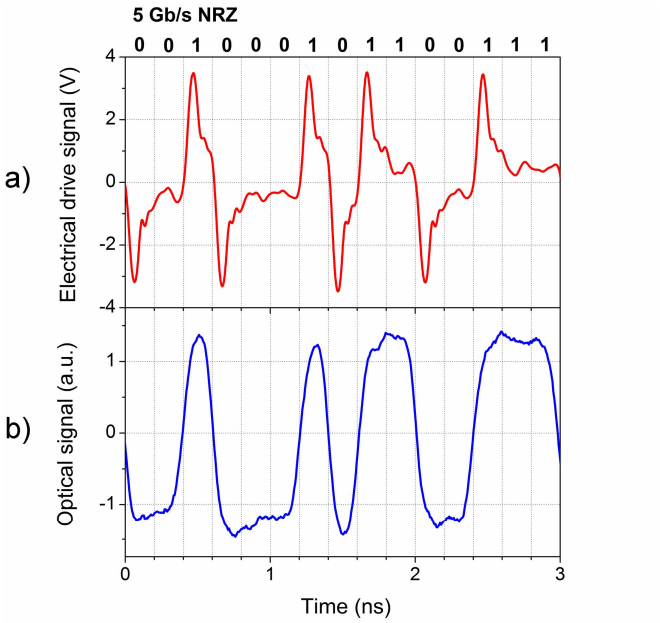

Fig. 3. (a). Pre-emphasized electrical drive signal at 5 Gb/s. Transitions between 0 and 1 bits have large amplitude, while consecutive 0's or 1's are suppressed. (b) Corresponding optical signal at the output of a L_{MZM} = 100 μm modulator.

#87799 - $15.00 USD Received 21 Sep 2007; revised 6 Nov 2007; accepted 7 Nov 2007; published 6 Dec 2007

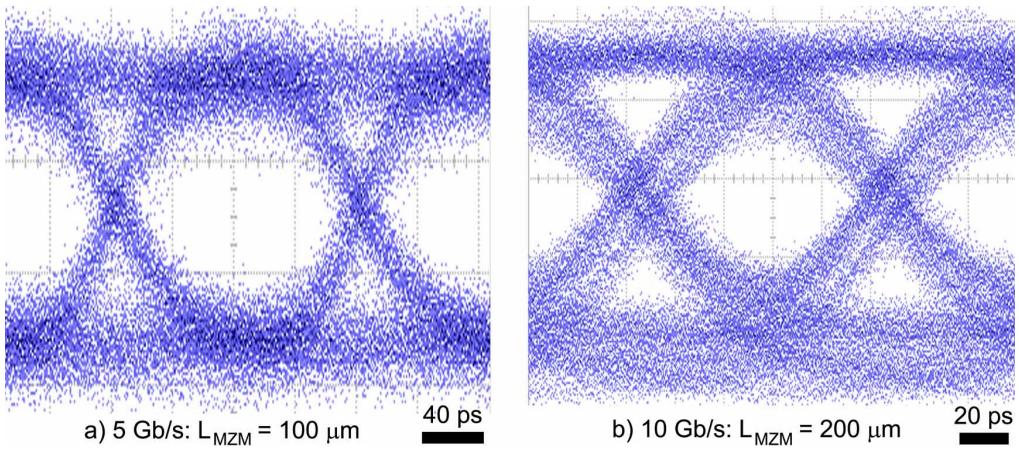

Fig. 4. Eyeline diagrams of NRZ optical data signals (PRBS 2^7-1) produced by several ultra-compact MZM devices. (a) L_{MZM} = 100 μm modulator operating at 5 Gb/s. (b) L_{MZM} = 200 μm modulator operating at 10 Gb/s.

Figure 4(a) contains an eyeline diagram of the modulated optical signal at the output of a 100 μm long MZM operating at 5 Gb/s (2^7-1 PRBS). Under these conditions, the device was biased at V_{bias} = 0.3 V, and drew a DC current of 2.17 mA. Given the p^+-i-n^+ diode forward resistance of 49 Ω (Fig. 1(b)), this corresponds to a DC power consumption of 230 μW. An additional RF average power of 41 mW was required for data transmission, calculated assuming a 49 Ω load driven by the 5 Gb/s pre-emphasized electrical waveform. Operation at 10 Gb/s was demonstrated using the increased optical modulation efficiency afforded by a longer 200 μm MZM device, as illustrated in Fig. 4(b). In this case, the modulator device was unbiased, drew a DC current of 2.69 mA under operating conditions, and consumed DC and RF power of 287 μW and 51 mW, respectively. The high-speed 10 Gb/s performance of the 200 μm long MZM represents a 25x improvement in demonstrated data rate in comparison with recent work in which a MZM of similar length (250 μm) and waveguide design was reported [24, 25].

Table 1: Comparison of power consumption for recently reported SOI optical modulators.

	DC operating conditions	**RF power consumption**
Cornell injection microring [10, 11]	18 to 105 μW[a]	–
Intel depletion MZM [15]	613 mW[b]	–
MIT injection MZM [24, 25]	10 mW[c]	100 to 200 mW for 10 GHz tone
IBM injection MZM	287 μW[d]	51 mW / 5 pJ/bit at 10 Gb/s

[a] ON-OFF switching power

[b] Bias power, estimated from published data

[c] Bias power

[d] DC component of operating power

As the above measurements illustrate, the RF power is by far the dominant contribution to the power dissipation. While this is true of most SOI optical amplitude modulators, the RF power is seldom reported in the literature, as shown in the device comparison compiled in Table 1. Most frequently, only the bias power, or the power required to switch the optical transmission from ON to OFF under DC conditions (i.e. no data transmission) is disclosed. In general, this figure severely underestimates the power required for high speed operation, and

#87799 - $15.00 USD Received 21 Sep 2007; revised 6 Nov 2007; accepted 7 Nov 2007; published 6 Dec 2007

does not present a realistic picture for link power budgeting purposes. For example, in order to compose metrics useful for comparing various high-bandwidth on-chip interconnect architectures (i.e. optical versus electrical), such as the energy required to transmit a single bit, a full tally of all power consumed by the modulator is needed. In comparison with the only report of RF power consumption of which the authors are aware [24, 25] (100 to 200 mW for a 10 GHz tone, also no data transmission), the 51 mW power consumption reported here for 10 Gb/s data transmission is superior, corresponding to a required energy per bit of approximately 5 pJ/bit. It is possible that a small fraction of this power is reflected from the p^+-i-n^+ diode due to impedance mismatch at high frequencies. Design of optimized on-chip termination loads may permit the energy per bit to be reduced further.

It is worthwhile noting that an optimized 100 μm long MZM of the present design may occupy a miniscule silicon footprint as small as 100 um x 10 um = 0.001 mm^2, this being only ~5x larger than the footprint occupied by a typical microring resonator modulator [10, 11]. In applications where the broadband optical performance and improved tolerance to on-chip temperature variations and fabrication process fluctuations are critical, the electrooptic MZM design presented here illustrates that suitable broadband SOI nanophotonic modulators can be realized without paying the prohibitively large footprint penalty conventionally associated with comparing non-resonant versus resonant modulator designs.

4. Conclusions

We have demonstrated SOI Mach-Zehnder electrooptic modulators having ultra-compact 100 to 200 μm long p^+-i-n^+ diode active regions, suitable for on-chip optical interconnect applications. The measured $V_\pi \cdot L$ figure of merit was 0.36 V-mm, this being a factor of 100 times smaller than previously reported for SOI MZM devices. This enhanced electrooptic efficiency originated from nearly complete free carrier/optical mode overlap in high-confinement nanophotonic rib waveguides. Using electrical pre-emphasis, NRZ optical modulation at data rates up to 10 Gb/s has been shown, with low RF power consumption of 51 mW or 5 pJ/bit.

Acknowledgments

The authors would like to thank Alexander Rylyakov, Clint Schow, and Dan Kuchta for providing instrumentation and valuable advice for pre-emphasis equalization measurements. This work was supported in part under DARPA contract N00014-07-C-0105.

#87799 - $15.00 USD Received 21 Sep 2007; revised 6 Nov 2007; accepted 7 Nov 2007; published 6 Dec 2007